Scientific Research Publishing

Open Journal of Geology, 2022, 12, 811-827
https://www.scirp.org/journal/ojg
ISSN Online: 2161-7589
ISSN Print: 2161-7570

Magnetic Facies and Polymetallic Sulphides Deposit in the Mafic and Ultramafic Intrusions of Samapleu (Western Côte d'Ivoire)

Simon Pierre Djroh[1*], Gnamba Emmanuel Franck Gouedji[2], Ehui Beh Jean Constantin Aka[1], Boko Célestin Sombo[1], Christian Picard[3], Marc-Antoine Audet[4], Bouaké Bakayoko[4]

[1]Applied Geophysics Research Team, Laboratory of Geology, Mineral and Energy Resources (LGRME), Faculty of Earth Science and Mineral Resources, Félix Houphouet Boigny University, Abidjan, Côte d'Ivoire
[2]Geology and Mining Sciences, University of Man, Man, Côte d'Ivoire
[3]University of Franche-Comté (UMR 6249), 16 Route de Gray, Besançon, France
[4]Sama Nickel-CI Sarl, 2 Plateaux Vallons, Abidjan, Côte d'Ivoire
Email: *djrohsp@gmail.com

How to cite this paper: Djroh, S.P., Gouedji, G.E.F., Aka, E.B.J.C., Sombo, B.C., Picard, C., Audet, M.-A. and Bakayoko, B. (2022) Magnetic Facies and Polymetallic Sulphides Deposit in the Mafic and Ultramafic Intrusions of Samapleu (Western Côte d'Ivoire). *Open Journal of Geology*, **12**, 811-827.
https://doi.org/10.4236/ojg.2022.1210039

Received: August 6, 2022
Accepted: October 28, 2022
Published: October 31, 2022

Abstract

Mafic and ultramafic intrusions observed in the Archean formations of the Sipilou region exhibit occurrences of polymetallic sulphide. Mapping, petrographic and geochemical studies have defined magnetic facies associated with the various geological units. The results of this work reveal that cupronickel sulphides, olivines and pyroxenes as well as spinels are related to ultrabasic formations where strong magnetic facies prevail. Iron sulphides and magnetite are linked to quartzo-feldspathic and jotunite-enderbite formations, which are characterised by moderate magnetic facies. The latter are thought to be derived from anatexite remobilisation within Archean granulites, which have weak magnetic facies.

Keywords

Magnetic Facies, Mapping, Petrography, Geochemistry, Sulphides, Côte d'Ivoire

1. Introduction

Copper-nickel sulphide deposits are generally associated with ultrabasic formations [1] [2]. Other types of deposits have developed in a sedimentary environment where bacteriological activities on biogenic sulphur concentrate metal-bearing ions from supergene alteration of ancient magmatic complexes [3]. In Côte d'Ivoire, mafic and ultramafic intrusions, including Sama Main (*SM*) and Extension 1 (E_1), have been observed within Archean formations in the Sipilou region where cup-

per-nickel occurrences have been described at Samapleu [2] [4] [5] [6] [7]. This work aims to study the relationships between different magnetic facies, geological formations and associated polymetallic sulphides in order to contribute to a better characterization of the metal concentrations at Samapleu.

2. Study Area and Geological Context

The study area is located approximately 7 km south of Samapleu, a village in the department of Sipilou in western Côte d'Ivoire (**Figure 1**). It lies between 856,400 to 859,315 North latitudes and 616,850 to 636,280 West longitudes. Its geology is associated with the Liberian orogeny [8] and consists of grey granulitic gneiss and pink granulite with local migmatization (**Figure 1**). Within this granitic basement, mafic units composed of gabbro and gabbro-norite, and ultramafic units represented by peridotite, pyroxenite and chromitite are found in intrusions [7] [9].

3. Analytical Methods

The methodological approach focuses on mapping, petrographic and geochemical characterisation of core samples from drillings. Located in a tropical zone, the Samapleu site is covered by a large lateritic layer through which few crystalline rocks outcrop. The mapping is mainly based on ground magnetic data and hammer prospecting. Application of Fast Fourier Transform (*FFT*) filters to the magnetic data produced maps of apparent magnetic susceptibility ($L(r,\theta)$) and Analytical Signal (*AS*) according to the following equations:

$$L(r,\theta)=\frac{1}{2\pi F\cdot H(r)\cdot\Gamma(\theta)\cdot K\cdot(r,\theta)} \quad \text{and} \quad AS=\sqrt{\left(\frac{\partial F}{\partial x}\right)^2+\left(\frac{\partial F}{\partial y}\right)^2+\left(\frac{\partial F}{\partial z}\right)^2}$$

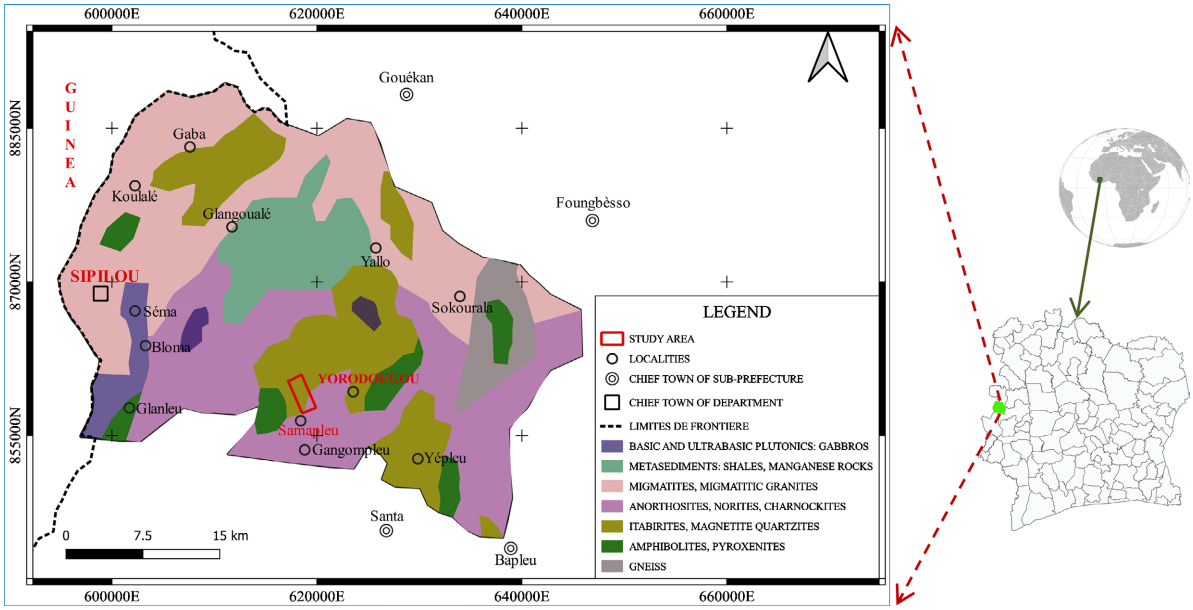

Figure 1. Study area and geological map [9].

$$\text{With}\quad H(r)=e^{-hr};\quad \Gamma(\theta)=\left[\sin Ia+i\cos I\cdot\cos(D-\theta)\right]^2\quad \text{et}$$

$$K(r,\theta)=\left[\frac{\sin(ar\cos\theta)\cdot\sin(ar\sin\theta)}{ar\cos\theta\cdot ar\sin\theta}\right]$$

where, H(r): downward continuation; $\Gamma(\theta)$: correction of the geometric effect; $K(r,\theta)$ Reduction to the pole; F: Total geomagnetic field; h: depth in ground units; I: geomagnetic inclination; I_a: pole reduction amplitude inclination; D: geomagnetic declination; θ: latitude; r: wavenumber.

The first ($L(r,\theta)$) provides information on the distribution of (acidic, basic and ultrabasic) units and thus facilitates geological interpretation. The second (*AS*) presents maximum amplitudes on the fault and/or contact and highlights discontinuities to discriminate magnetic facies linked to the ferromagnesian oxide's distribution in the rock matrix [10].

The petrographic and geochemical characterization of the formations is based on the sampling method and analytical techniques. To do this, samples of the *SM* and E_1 intrusions as well as the surrounding rocks were taken from the drill holes for the production of polished thin sections. The silicate minerals in these rocks were studied under transmitted light with *Zeiss AXIOSKOP* 40 and *Leica* microscopes. Sulphides and oxides were also observed with a *Leica DMLM* microscope in reflected light. The geochemical study involved a total of 18 samples from the boreholes whose 10 came from the intrusions (*SM* and E_1) and 8 from the surrounding rocks. They were conditioned according to the methods of [11], then melted with lithium metaborate ($LiBO_2$) and dissolved in nitric acid (HNO_3). Major elements were analysed by optical emission spectrometry (*ICPOES Icap* 6500) with radial flare. And lastly, minor and rare earth elements were analysed by mass spectrometry (*ICP-MS X7* from Thermo).

4. Results

4.1. Mapping

The magnetic susceptibility (k) map shows three (3) domains that provide information on the acidity of the rocks and help in the mapping (**Figure 2(a)**). The first domain is characterised by low k values ($k \leq 0.152$) and reflects, at low latitudes, the magnetic response of formations rich in ferromagnesian minerals. It is superimposed with the outcrops of mafic and ultramafic rocks that constitute the E_1 and *SM* intrusions. The second domain is marked by high k values ($k \geq 0.162$) and corresponds, in our tropics, to the signature of quartzo-feldspathic rocks relatively poor in ferromagnetic minerals. This domain covers a large part of the prospect and is superimposed on the granulite corps. Between these two entities, there is a domain characterised by intermediate values of magnetic susceptibility which are marked by the yellow-orange colour. This domain corresponds to the magnetic response of formations relatively rich in magnetite (**Figure 2(a)** and **Figure 2(c)**). The analytical signal map discriminates the domains into four (4) magnetic facies that are related to the geological structures (**Figure 2(b)**).

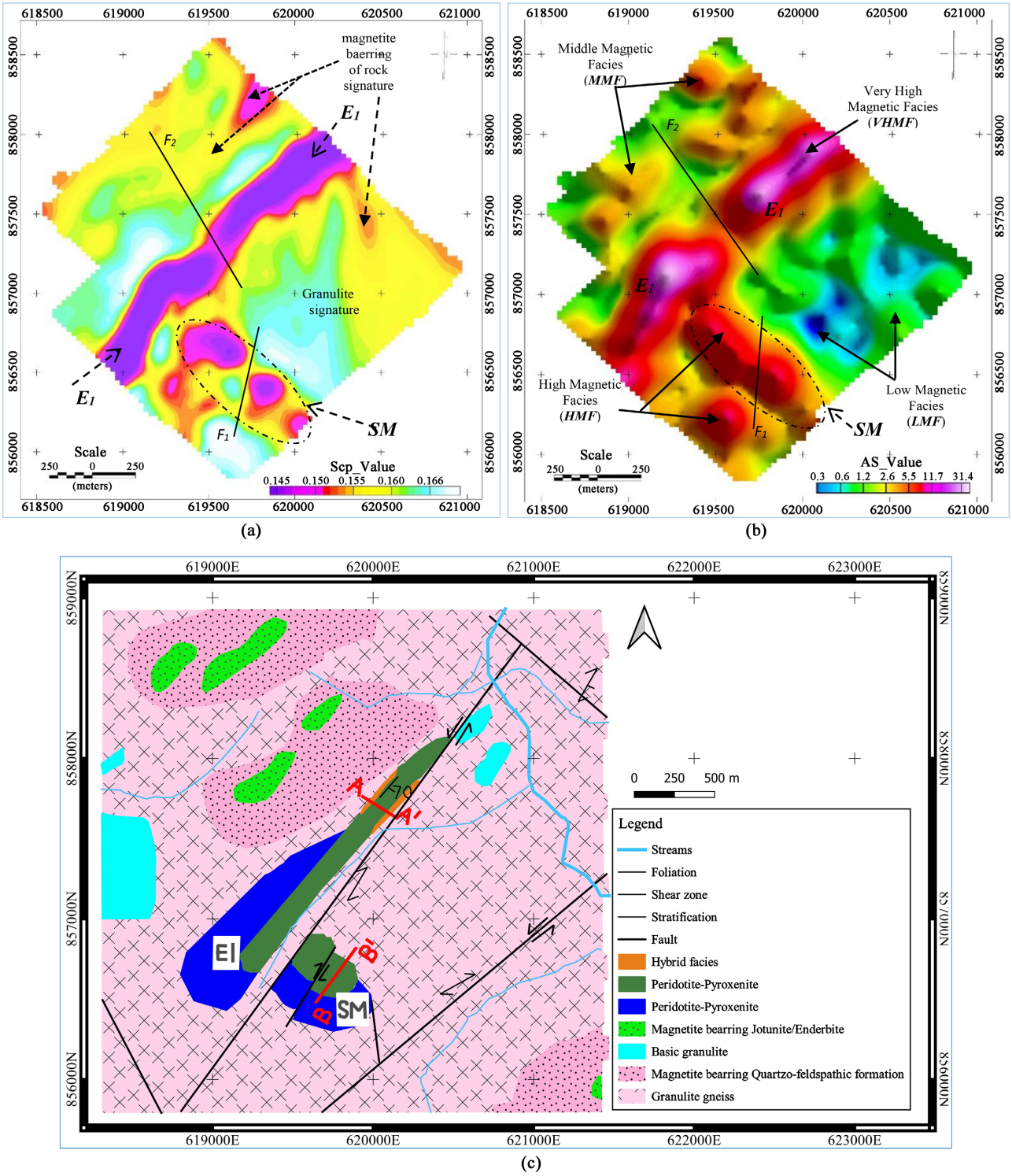

Figure 2. Geophysical and geological map. (Extension 1 = E_1; Samapleu Main = *SM*). (a) Apparent susceptibility of magnetic field [6]. (b) Analytical signal of magnetic field [6]. (c) Samapleu schematic geological map [12].

Thus, the very high magnetic facies (*VHMF*) reflect a strong basic signature and has a NE-SW orientation. Its axis shows some distortions and is interrupted by NW-SE oriented F_2 fault.

The high magnetic facies (*HMF*) have two (2) main directions. It borders the *VHMF* laterally in a NE-SW direction and, to the south of the prospect, has a NW-SE orientation. To the northwest and southeast, the low magnetic facies (*LMF*) does not seem to define a preferred orientation but rather corresponds to the magnetic response of the pre-existing basement. In the north-western part of this complex, moderate magnetic facies (*MMF*) are observed in places, with a reduced lateral extension, but mainly oriented NE-SW (**Figure 2(b)**).

The superposition of magnetic facies and geological hammer observations allow to connect the peridotites/pyroxenites response to the *VHMF* and the gabbro-norites to the high magnetic facies (*HMF*). These two facies define the mafic-ultramafic sequence of the E_1 intrusion. It is elongated in a NE-SW direction over a length of about 2 km and a width of 50 to 200 meters, dipping 70˚ to 80˚ to the South East, parallel to the major gneissic foliation. The E_1 intrusion shows some distortions due to the effects of fractures whose main one being F_2 and trending NW-SE (**Figure 2(b)**).

To the south of the prospect, the intrusion of Sama Main (*SM*) is characterised only by the high magnetic facies (*HMF*), which reflects the magnetic response of the gabbro-norite. It is less elongated, subrounded and oriented NW-SE with a subvertical dip trending NE.

However, the apparent magnetic susceptibility map indicates at the *SM* intrusion level, in addition to the basic units, the magnetic signature of the acidic rocks (**Figure 2(a)**).

Similarly, the geological map also notes the existence of peridotites and/or pyroxenites on its northern margins (**Figure 2(c)**). These controversies between the high magnetic facies (*HMF*) and the geological units within the *SM* intrusion will be highlighted with the results of petrographic and geochemical studies. The moderate magnetic facies (*MMF*) is associated with quartzo-feldspathic formations and jotunite/enderbite assemblages that locally concentrate ferromagnesian minerals. They occur to the northwest and south of the prospect and are mainly NE-SW trending.

The low magnetic facies (*LMF*) is the signature of the Archean granulite assemblages. Although having a homogeneous structure in places, it's characterised by a gneissic structure frequently marked by early foliations of variable direction with a strong dip of 70˚ to 90˚ towards the South East or North West [12].

4.2. Petrography

4.2.1. Rock Formations

Two sets of rocks are recorded on the prospect, namely country rocks and the Samapleu's mafic-ultramafic intrusions (*SM* and E_1).

The host rocks include more or less gneissic granulites, jotunite/enderbite assemblage and quartzo-feldspathic formations.

Gneissic granulites may have a foliated (**Figure 3(a)**) or equant structure. They are massive, generally with a granoblastic to grano-nematoblastic texture.

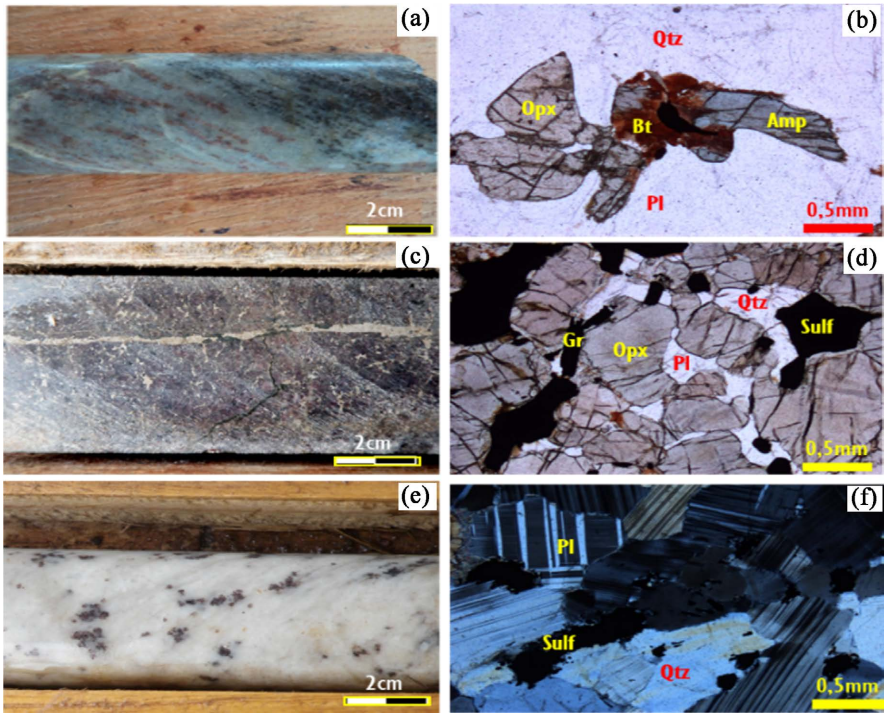

Figure 3. Macrophotography and microphotography of surrounding rocks. (a) Macroscopic aspect of a gneissic granulite; (b) Granulite seen in unanalysed polarised light (*LPNA*); (c) Macroscopic aspect of a sulphide jotunite; (d) Jotunite seen in *LPNA*; (e) Macroscopic aspect of a quartzo-feldspathic formation; (f) Quartz-feldspathic formation seen in polarised light analysis (*LPA*). Qtz = quartz; Pl = plagioclase; Opx = orthopyroxene; Amp = amphibole; Bt = biotite; Gr = graphite; Sulf = sulphide.

From the mineralogical viewpoint, they are mainly composed of orthopyroxene (Opx), oligoclase, quartz and biotite in variable proportions. Quartz (40% to 50%) is very variable in size and has an undulating extinction. Oligoclase (25% to 35%) often contains exsolutions of potassium feldspar. Opx (bronzite), which represents 20% to 30% of the rock, is of medium-sized (0.1 to 0.3 mm) with some porphyroblastic crystals (4 mm to 1 cm). It has a biotite or amphibole reaction crown (Figure 3(b)) in places. Ilmenite, as well as sulphides (pyrite and pyrrhotite), appear in small proportions (≤2%) and zircon is incidental.

The jotunite-enderbite assemblage indicates a decimetric to metric interstratification with paragneiss and quartzo-feldspathic formations. It is green in colour with brownish-purple flecks and is massive (Figure 3(c)). The constituent minerals are medium to coarse in size (0.2 - 8 mm) and have a granoblastic texture under microscopic observation.

Opx (hypersthene, 50% - 70%) is locally transformed into amphibole (cummingtonite). Garnet has a proportion of 5% - 10% in the rock. Amphibole and biotite are locally coronitic (Figure 3(d)). In these rocks, magnetite is relatively present in places. The jotunite-enderbite set contains more than 10% sulphides (pyrite, pyrrhotite and chalcopyrite) generally disseminated or in the form of veins, with locally tapered graphite (size ≤ 1 mm) (Figure 3(c) and Figure 3(d)).

Quartzo-feldspathic formations are massive and whitish with brown or

green flecks (Figure 3(e)). Microscopically, it is enriched in quartz, plagioclase and secondarily in hypersthene, garnet, biotite and amphibole (Figure 3(f)). In places, quartz (0.1 mm to 1 cm) reaches up to 40% to 70% of the rock and feldspar (plagioclase) is between 10% and 30%. Like garnet, hypersthene is locally around 10%. Biotite and amphibole are less than 7%. This rock contains less than 5% of sulphides (pyrite, pyrrhotite) generally disseminated, with locally high proportion of graphite and magnetite in places.

The mafic and ultramafic intrusions concern the *SM* and E_1 zones. They are quite similar and all have cumulative textures. They are grouped into two units, one of which, ultramafic, is made up of peridotites and pyroxenites, and the other mafic is made up of norite, gabbro-norite and anorthosite.Within the ultramafic unit, the peridotite consists mainly of weakly serpentinised lherzolite and secondarily of harzburgite and dunite. It is massive, very magnetic and blackish-green in colour (Figure 4(a)). In places it is banded with serpentine and weakly mineralised with sulphide. Microscopically, it is composed of olivine, serpentine, Opx, clinopyroxene (Cpx), amphibole, spinel and sulphide (Figure 4(b)). The olivine (70% - 90% of the rock) is cumulus-shaped, sub-rounded and has minerals of 0.1 - 3 mm in diameter. Serpentine (3% to 4%) borrows the olivine's fissure networks and is associated with magnetite. Opx and Cpx represent less than 15% of the rock. Green amphibole (5% to 20%) is interstitial between

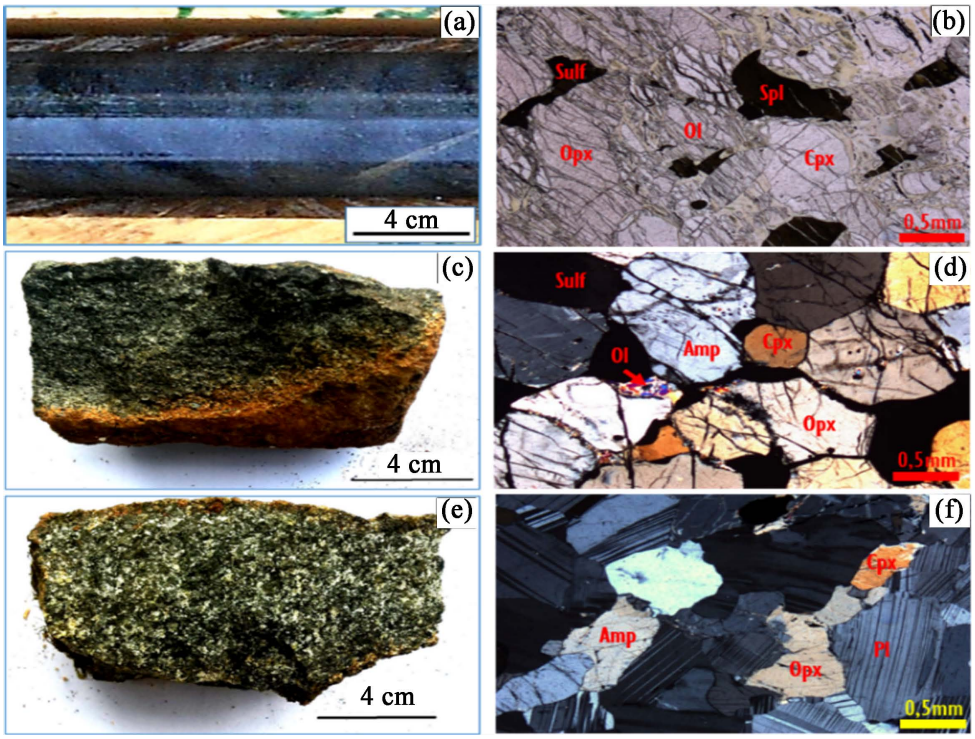

Figure 4. Macrophotography and microphotography of the rocks of the Samapleu intrusions. (a) Macroscopic aspect of a peridotite; (b) Peridotite seen in LPNA; (c) Macroscopic aspect of a pyroxenite; (d) Pyroxenite seen in LPA; (e) Macroscopic aspect of a gabbro-norite; (f) Gabbro-norite seen in polarised light analysis (LPA). Ol =olivine; Spl = spinel; Opx = orthopyroxene; Cpx = clinopyroxene; Amp = amphibole; Pl = plagioclase; Sulf = sulphide.

the olivine crystals. Sulphides and spinels represent less than 5% of the rock.

Pyroxenites are composed of pyroxenite in the strict sense (ss), olivine pyroxenite and plagioclase pyroxenite. They are massive, green speckled with brown, locally magnetic and strongly mineralised in sulphide (**Figure 4(c)**). Microscopically, they consist of Opx and Cpx, amphibole and plagioclase, olivine, spinel and sulphides in variable proportions (**Figure 4(d)**). Opx is more abundant (more than 60% of the rock) than Cpx, which makes less than 15% of the rock. Amphibole and plagioclase are 10% - 15% of the rock and are xenomorphic to sub-automorphic. Olivine is less abundant and spinels are interstitial in the pyroxenes. Sulphides are abundant and approach 50% in the pyroxenites (**Figure 4(c)**).

The mafic unit is massive and whitish-grey with brown flecks (**Figure 4(e)**). It is magnetic and weakly mineralised in sulphide. Microscopically, this unit is composed of Opx and Cpx, plagioclase and amphibole, biotite and sulphide in variable proportions (**Figure 4(f)**). Opx (5% - 40% of the rock) is subrounded and variable in size (3 mm to 1 cm). Cpx (≤15%) has a very heterogeneous distribution and locally favours norite formation. Plagioclase is quite abundant (30% - 40%) and variable in size (0.1 - 5 mm). Of variable shape, it is interstitial to the pyroxenes. Its proportion reaches locally 80% to 90% of the rock and forms the anorthosite. The association of plagioclase with pyroxenes gives in places a biotite reaction crown. Amphibole (5% - 10%) is xenomorphic and interstitial between pyroxenes and plagioclase. Oxides and sulphides are small and less abundant in the rock (0% - 5%).

4.2.2. Iron Oxide and Sulphide Mineralization

In the host rocks, iron oxides consisting of magnetite are contained in the jotunite/enderbite assemblage as well as the quartzo-feldspathic formations. In the jotunites/enderbites, magnetite (Fe_3O_4) is relatively present in places in sub-rounded and disseminated form. In the quartzo-feldspathic formations, it forms a banded alternation with a foliated structure (**Figure 5(a)**). Sulphides are generally less abundant within these rocks. They are disseminated and consist mainly of pyrrhotite, pyrite and secondarily of chalcopyrite (**Figure 5(b)**).

On the other hand, in the mafic and ultramafic intrusions (*SM* and E_1), the oxides observed are mainly spinels ($MgAl_2O_4$) and magnetite in relatively small quantities. On the other hand, sulphides are abundant in the ultramafics, particularly in the pyroxenites, where they are globally disseminated, interstitial and in places form massive and brecciated sulphides (**Figure 5(c)**). They are mainly composed of pyrrhotite, pentlandite, chalcopyrite and secondarily of pyrite (**Figure 5(d)**).

4.3. Geochemistry

4.3.1. Host Rocks

Major element contents in the gneissic granulite are characterised by high contents of non-magnetic oxides [SiO_2 (65.85% to 70.21%) & Al_2O_3 (14.49% to

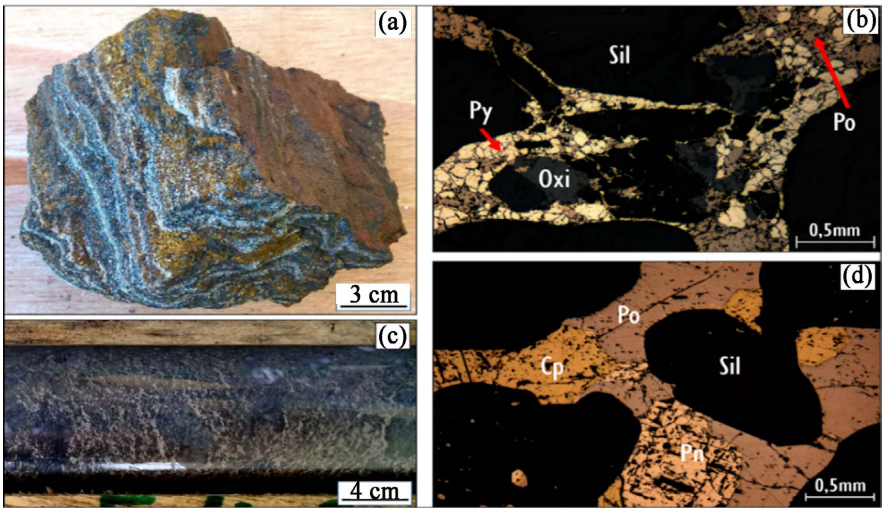

Figure 5. Macrophotography and microphotography of iron oxide and sulphide mineralisation of the Samapleu lithologies. (a) Macroscopic aspect of a magnetite-banded quartzo-feldspathic formation; (b) Sulphide paragenesis (pyrrhotite, pyrite) of a jotunite; (c) Macroscopic aspect of a brecciated sulphide pyroxenite; (d) Sulphide paragenesis (pyrrhotite, chalcopyrite, pentlandite) of a pyroxenite. Sil = silicate; Oxi = oxide; Po = pyrrhotite; Py = pyrite; Cp = chalcopyrite; Pn = pentlandite.

16.99%)] and low contents of magnetic oxides [Fe_2O_3 (2.98% to 4.94%) & MgO (1.42% to 2.85%)]. In the quartzo-feldspathic magnetite formations, grades are relatively high for both non-magnetic oxides [SiO_2 (53% - 59%) & Al_2O_3 (13%)] and magnetic oxides [Fe_2O_3 (19 and 25%) & MgO (3% and 4%)].

The chemical analysis of the enderbite and jotunite shows similar contents of magnetic and non-magnetic oxides with a slight increase in alumina, for the enderbite, and magnesia for the jotunite. The contents of CaO, Na_2O and K_2O, MnO and TiO_2 as well as some minor elements (Ni, Cr and Co) are generally low (Table 1).

The rare earth spectra (*REE*) of the host rocks are mainly enriched with the (*La/Yb*)*n* ratio varying between 4.57 and 217.13 except for the jotunite where the (*La/Yb*)*n* ratio is 0.73 (Figure 6).

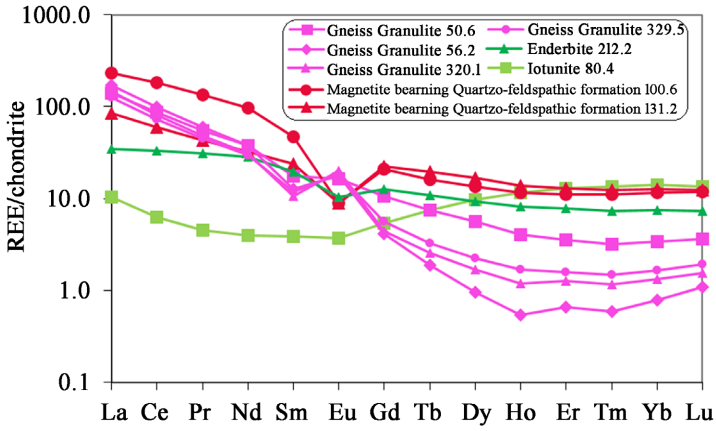

Figure 6. Rare earth contents (*REE*) of host rocks normalised to chondrite [14].

Table 1. Major element (%) and rare earth element (ppm) composition of host rocks.

Drilling	SM13-509544				SM24-645670	SM24-661614		
Lithology	Jotunite	Enderbite	Quartzo-feldspathic magnetite formation		Gneissic granulite [12]			
Samples	SM13/80.4	SM13/212.2	SM13/100.6	SM13/131.2	SM24 (3) /50.6	SM24/56.2	SM24/320.1	SM24/329.5
Oxides (%)								
SiO_2	41.10	45.20	58.93	53.39	65.85	70.21	68.86	70.18
TiO_2	0.20	0.31	0.46	0.36	0.50	0.45	0.46	0.42
Al_2O_3	5.63	9.65	13.59	13.49	16.99	15.71	16.50	14.49
Fe_2O_3	36.20	37.89	19.28	25.54	4.94	2.98	3.55	3.18
MnO	0.23	2.46	0.25	0.33	0.06	0.02	0.04	0.04
MgO	13.10	2.92	4.92	3.69	2.85	1.52	1.37	1.43
CaO	0.67	2.29	1.09	1.85	2.73	2.88	3.68	3.11
Na_2O	0.29	bd	0.52	bd	4.67	5.10	5.00	4.30
K_2O	0.07	bd	0.17	0.02	0.76	1.17	0.94	1.21
P_2O_5	ld	0.08	0.04	0.07	0.09	0.04	0.06	0.07
PF	1.38	−2.13	−0.47	−0.17	−0.03	0.57	0.43	1.40
Total	**98.86**	**98.66**	**98.78**	**98.56**	**99.39**	**100.65**	**100.89**	**99.84**
Trace elements en (ppm)								
Ni	800.40	68.28	164.10	152.00	21.13	ld	ld	12.87
Co	119.80	15.14	26.98	27.17	11.79	9.13	11.19	8.51
Cr	1708	137.40	323.60	252.20	56.21	28.34	32.38	33.06
Cu	718.30	34.79	122.30	66.24	56.00	170.40	164.30	91.04
La	2.54	8.46	57.09	20.83	34.17	41.59	35.59	30.71
Ce	3.99	21.04	116.60	37.87	54.67	63.06	51.42	46.48
Pr	0.44	2.99	12.92	4.14	5.28	5.71	4.61	4.34
Nd	1.87	13.55	45.79	15.43	17.74	17.76	14.72	14.03
Sm	0.59	3.02	7.25	3.65	2.73	1.95	1.65	1.84
Eu	0.21	0.61	0.52	0.52	0.95	1.05	1.15	1.07
Gd	1.10	2.60	4.30	4.54	2.17	0.86	0.91	1.16
Tb	0.28	0.40	0.61	0.74	0.28	0.07	0.09	0.12
Dy	2.48	2.36	3.41	4.29	1.42	0.24	0.43	0.57
Ho	0.65	0.47	0.66	0.79	0.23	0.03	0.06	0.10
Er	2.15	1.29	1.85	2.15	0.59	0.11	0.21	0.26
Tm	0.35	0.19	0.28	0.32	0.08	0.02	0.03	0.04
Yb	2.35	1.25	1.93	2.09	0.56	0.13	0.22	0.27
Lu	0.35	0.19	0.30	0.32	0.09	0.03	0.04	0.05
(La/Sm) n	2.71	1.76	4.95	3.59	7.87	13.39	13.57	10.48
(La/Yb) n	0.73	4.57	19.96	6.72	41.02	217.13	110.46	76.04
(Dy/Yb) n	0.69	1.23	1.15	1.34	1.64	1.22	1.30	1.36

bd = belon detection.

The light rare earths (*LREE*) show an enrichment of 10 to 100 times higher than that of chondrite, with a (*La/Sm*)*n* ratio between 1.76 and 13.57, indicating depressed spectra. The heavy rare earths (*HREE*) spectra are relatively flat around 1 to 10 times the chondrite contents with a (*Dy/Yb*)*n* ratio between 0.69 and 1.64. Both a positive and negative Eu anomaly due to feldspar enrichment is observable [13]. The spectra suggest a calc-alkaline affinity.

4.3.2. Mafic and Ultramafic Intrusions (SM and E_1)

The major elements of the mafic and ultramafic rocks (*SM* and E_1) are characterised by highly variable contents, characteristic of rocks composed of cumulates. Indeed, they have low non-magnetic oxide contents [SiO_2 (38.94% to 51.91%) & Al_2O_3 (2.65% to 19.20%)] and high magnetic oxide contents for the magnesian pole [MgO (10.59% to 32.52%)], the iron pole being relatively low [Fe_2O_3 (7.21% to 16.50%)].

Oxide contents (magnetic and non-magnetic) in the mafic rocks are slightly lower than in the ultramafic rocks. However, there is an enrichment of calcium [CaO (1.98% to 13.86%)] within the mafic rocks.

In addition, it is revealed that overall; the contents of Na_2O, K_2O, MnO and TiO_2 are extremely low, below 2%.

Some minor elements such as Ni (238 to 2374 ppm), Cr (695 to 9428 ppm), Cu (46 to 1004 ppm) and Co (42 to 168 ppm) have moderately high contents (**Table 2**).

The rare earth spectra are globally flat for all the *SM* and E_1 intrusive rocks, with a (*La/Yb*)*n* ratio that varies from 0.35 to 3.67. These rocks show a low enrichment, 1 to 10 times, compared to the chondrite content (**Figure 7**). They are slightly enriched in light rare earths (*LREE*) with a (*La/Sm*)*n* ratio varying from 0.43 to 3.32, and relatively constant in heavy rare earths (*HREE*) with the (*Dy/Yb*)*n* ratio ranging between 0.73 and 1.14. The positive Eu anomaly in gabbro-norite, plagioclase pyroxenite is related to the abundance of plagioclase within these rocks (**Table 2**).

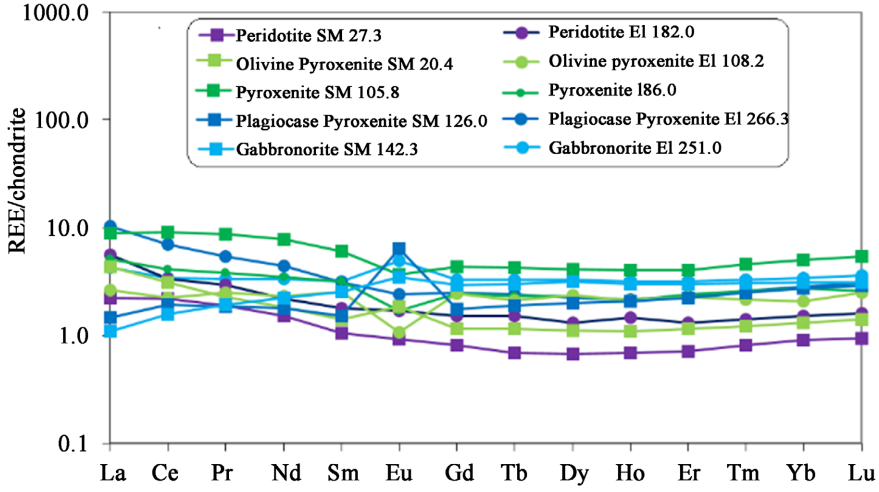

Figure 7. Rare earth contents (REE) of the *SM* and E_1 intrusions normalised to chondrite [14].

Table 2. Major element (%) and rare earth element (ppm) composition of the *SM* and *E*i intrusions.

Drilling	Extension 1/SM24-661614 [12]					Samapleu Main/SM44 450250b				
Lithology Samples	Lherz SM24 /182	Ol Web SM24 /108.2	Web SM24 /186	Pl Web SM24 /266.3	Gab-nor SM24 /251	Lherz SM44(b) /27.3	Ol Web SM44(b) /20.4	Web SM44(b) /105.75	Pl Web SM44(b) /126	Gab-nor SM44(b) /142.3
Oxides (%)										
SiO_2	38.94	43.63	43.47	49.67	46.67	41.34	40.21	50.91	45.38	47.77
TiO2	0.12	0.20	0.18	0.16	0.22	0.05	0.11	0.24	0.23	0.20
Al_2O_3	2.65	6.68	7.86	7.05	19.20	3.25	9.03	6.51	11.37	15.72
Fe_2O_3	16.21	15.68	13.75	14.59	7.50	15.90	15.21	14.44	12.42	7.50
MnO	0.24	0.19	0.15	0.22	0.13	0.20	0.18	0.25	0.17	0.15
MgO	32.52	27.33	23.78	23.97	10.59	30.48	26.41	21.61	19.69	12.91
CaO	3.10	3.86	4.77	2.87	12.13	1.98	4.81	4.67	7.68	13.86
Na_2O	0.20	0.28	0.37	0.28	1.58	0.31	0.63	0.32	1.07	0.84
K_2O	0.05	0.05	0.06	0.11	0.15	0.10	0.09	0.07	0.10	0.01
PF	4.65	−0.08	3.64	0.43	1.03	5.10	0.73	−0.37	0.63	0.37
Total	**98.67**	**97.81**	**98.02**	**99.35**	**99.21**	**98.69**	**97.41**	**98.65**	**98.74**	**99.33**
Trace elements en (ppm)										
Ni	2094.00	1649.00	1288.00	1057.00	252.40	2374.00	1539.00	695.20	693.30	238.70
Co	168.10	134.80	112.50	79.90	42.19	152.80	145.70	87.16	88.42	45.84
Cr	6927.00	9428.00	8689.00	3414.00	695.60	1233.00	8681.00	2322.00	1797.00	955.50
Cu	233.60	284.90	949.20	1004.00	46.75	678.30	272.40	433.90	92.98	141.70
La	1.37	0.65	1.24	2.54	1.04	0.55	1.05	2.16	0.36	0.27
Ce	2.15	1.42	2.63	4.50	2.18	1.40	1.99	5.81	1.23	1.00
Pr	0.28	0.24	0.37	0.52	0.32	0.18	0.22	0.84	0.18	0.19
Nd	1.04	1.09	1.65	2.09	1.59	0.72	0.86	3.73	0.84	1.06
Sm	0.28	0.39	0.49	0.48	0.49	0.16	0.22	0.93	0.24	0.39
Eu	0.10	0.06	0.10	0.14	0.29	0.05	0.11	0.21	0.37	0.20
Gd	0.31	0.50	0.50	0.51	0.67	0.17	0.24	0.88	0.36	0.60
Tb	0.06	0.08	0.09	0.09	0.12	0.03	0.04	0.16	0.07	0.11
Dy	0.34	0.60	0.59	0.57	0.83	0.17	0.28	1.05	0.51	0.81
Ho	0.08	0.12	0.12	0.12	0.18	0.04	0.06	0.23	0.12	0.17
Er	0.22	0.38	0.40	0.39	0.52	0.12	0.19	0.67	0.37	0.50
Tm	0.03	0.05	0.06	0.07	0.08	0.02	0.03	0.12	0.06	0.08
Yb	0.25	0.34	0.45	0.47	0.57	0.15	0.22	0.84	0.45	0.51
Lu	0.04	0.06	0.07	0.08	0.09	0.02	0.04	0.14	0.07	0.08
(La/Sm) n	3.10	1.05	1.61	3.32	1.34	2.11	3.03	1.46	0.95	0.43
(La/Yb) n	3.67	1.28	1.87	3.62	1.24	2.44	3.30	1.74	0.54	0.35
(Dy/Yb) n	0.87	1.14	0.86	0.78	0.95	0.74	0.85	0.82	0.73	1.03

Peridot = peridotite, Ol = Olivine, Pyr = Pyroxenite, Pl = Plagioclase, Lherz = Lherzolite, Web = Webstérite, Gab-nor = Gabbronorite.

5. Discussion

5.1. Host Rocks and Magnetic Facies

The host rocks consist of gneissic granulites interspersed with quartzo-feldspathic formations and the jotunite-enderbite assemblage, which are locally magnetic and sulphurous. The gneissic granulites are essentially composed of cardinal minerals (oxides: Si/Al/Ca) and secondarily of ferromagnesian minerals (oxides: Fe/Mg) with respect to their geochemical compositions (see **Table 1**). This composition, which gives them weak magnetic facies (*LMF*), is a characteristic of acid rocks [12] [15] (see **Figure 2(a)**, **Figure 2(b)** and **Figure 2(c)**).

Within these granulites, moderate magnetic facies units appear in places, superimposed on quartzo-feldspathic and magnetite jotunite-enderbite formations (see **Figure 2(b)** and **Figure 2(c)**). The latter concentrate, locally compared to the granulites, an enrichment in magnetic oxides (oxide: Fe/Mg) coupled with a relative depletion in non-magnetic oxides (oxide: Si/Al) (see **Table 1**). This inverse evolution of oxide contents amplifies their magnetic response compared to granulites. This explains the presence of moderate magnetic facies (MMF) patches within the low magnetic facies (*LMF*) that characterises the gneissic granulites of Samapleu (see **Figure 2(b)** and **Figure 2(c)**). The granoblastic and granonematoblastic textures observed within these rocks suggest that they are affected by a high-grade metamorphism (granulite facies), dated to the Liberian (2.8 Ga) that characterises the Archean domain in Côte d'Ivoire [8] [12] [16] [17] [18] [19] [20].

The high SiO_2 and Al_2O_3, medium CaO and Na_2O contents on the one hand, and the overall enrichment in light rare earths (*LREE*) on the other hand, show that these rocks come from the continental crust [13] [21]. With regard to the structures (textures, foliation, etc.) and age (2.8 Ga), the quartzo-feldspathic and jotunite-enderbite formations, with locally iron sulphide-rich magnetite (pyrite, pyrrhotite), are thought to have formed by anatexis of the Archean gneissic granulitic crust during the Liberian orogeny [12] [22] [23] [24] [25].

5.2. Mafic to Ultramafic Intrusions and Magnetic Facies

The mafic and ultramafic rocks are intrusive within the Achaean crustal rocks. In Samapleu, they form two units, the Sama Main (*SM*), which is subrounded and oriented NW-SE and the Extension 1 (E_1), which is 50 to 200 m wide and about 2 km long in a NE-SW direction (see **Figure 2(b)**). They comprise continuous mafic and ultramafic horizons composed of gabbronorite-norite and peridotite-pyroxenite respectively, which are made up of olivine, pyroxene and amphibole cumulates.

The mapping reveals a clear correlation, at the level of the E_1 intrusion, between the magnetic facies and these lithologies. The gabbro-norites are superimposed on the high magnetic facies (*HMF*) and occupy the edges of the peridotite-pyroxenites, which are associated with the very high magnetic facies (*VHMF*) (see **Figure 2(a)**, **Figure 2(b)** and **Figure 2(c)**). However, at the level

of the *SM* intrusion, two controversies develop, on the one hand, by high magnetic facies which, on the other hand, is associated with gabbro-norites and peridotite-pyroxenites; and on the other hand, by the magnetic signature of acid rocks. The first is linked to a slight decrease in the magnetic oxide (MgO) content of the pyroxenes and olivines of the *SM* intrusion compared to E_1 (see **Table 2**). This causes the magnetic spectrum of the peridotites-pyroxenites to drop to that of the gabbronorites-norites in the *SM*. The second is related to a slight increase in oxide contents, magnetic (MgO) and non-magnetic [SiO_2 and CaO], in the gabbro-norites of the *SM* intrusion compared to E_1 (see **Table 2**). Indeed, the increase in [SiO_2 and CaO] attenuates the global magnetic response of the gabbro-norites, which, in the vicinity of the peridotite-pyroxenites, appear with a low magnetic response that characterises acidic rocks (see **Figure 2(a)**). Also, the increase in magnesia (MgO) content in the gabbro-norites contributes, at the level of the *SM* intrusion, to the conservation of the magnetic spectrum of these mafic rocks in the high magnetic facies (*HMF*).

The mineralogy and crystallochemistry of the *SM* and E_1 intrusions indicate that they are derived from a magma of mantle origin by fractional crystallisation [26].

The parallel spectra observed on the rare earths indicate a common source of the *SM* and E_1 formations (see **Figure 7**). They indicate moderate *LREE* enrichment and flat *HREE* spectra that would mark a mantle and crustal plume related origin [12] [27] [28] [29] [30].

Furthermore, the sulphide copper-nickel mineralization associated with these intrusions is magmatic in nature, formed by immiscibility of an early sulphide fluid from one or more silicate mafic and ultramafic magmas [12] [31] [32] [33]. These Samapleu intrusions are dated at 2.09 Ga (U-Pb age on rutile; Eburnian) and are, according to [5] contemporary with certain Birimian geodynamic events. They are thought to have been emplaced through fractures in a granulitic Achaean basement [2] [6] [12] [30].

6. Conclusion

The present study allows to link the high magnetic facies to the mafic and ultramafic intrusions, *SM* and E_1, which are made up of gabbronorite-norite-anorthosite and peridotite-pyroxenite respectively. These rocks are rich in copper-nickel sulphides (pyrrhotite, pentlandite and chalcopyrite), particularly in the pyroxenites where they are globally disseminated, interstitial and in places form massive and brecciated sulphides.

The *SM* and E_1 intrusions are of mantle origin, Eburnian in age (2.09 Ga; U-Pb age on rutile) and thought to have been emplaced through fractures within granulitic Achaean basement, which is linked to weak magnetic facies. The magnetite formations, composed of quartzo-feldspathic and jotunite-enderbite units, are associated with moderate magnetic facies. They are thought to be subordinated to anatexic mineral remobilization and have a low concentration of iron

sulphides (pyrite and pyrrhotite). They are nickel-free and have a crustal origin with a Liberian age (2.8 Ga; U-Pb age on Zircon).

This study linked cupper-nickel sulphides to strong magnetic facies created by magnetite, spinel, olivine and pyroxene. On the other hand, iron sulphides present locally in quartzo-feldspathic rocks are rather associated with moderate magnetic facies caused by magnetite. This approach, which allows the characterization of the polymetallic sulphides deposit environment, could be exported to other regions with similar geological formations.

Funding

No funding was provided for this study.

Acknowledgements

The authors are grateful to the General Management of Sama Nickel CI for agreeing to make the field study data available to us for this academic project.

Conflicts of Interest

All authors have read and agreed to submit this work to a scientific publication journal. The authors declare no conflicts of interest.

References

[1] Barnes, S.J. and Lightfoot, P.C. (2005) Formation of Magmatic Nickel Sulphide Deposits and Processes Affecting Their Copper and Platinum Group Element Contents. In: Hedenquist, J.W., Thompson, J.F.H., Goldfarb, R.J. and Richards, J.P., Eds., *Society of Economic Geologists* 100*th Anniversary Volume*, Society of Economic Geologists, Littleton, 179-213. https://doi.org/10.5382/AV100.08

[2] Ouattara, N. (1998) Petrology, Geochemistry and Metallogeny of Sulphides and Platinum Group Elements from Côte d'Ivoire Ultrabasites. PhD Thesis, University of Orléans, Orléans, 186 p.

[3] Okitaudji, L.R. (2001) Formation Model of the Shaba Copper-Cobalt Deposits in the Democratic Republic of Congo. *Bulletin of Earth Academia of Lorraine*, **40**, 19-40.

[4] Angoran, Y.E. (1978) Geophysical Prospecting by Magnetometry and Induced Polarization (IP) at Samapleu (Yorodougou). Société pour le Développement Minier de la Côte d'Ivoire, Abidjan, Report No. 441, 2-10.

[5] Tahua, A and Sahy, L. (1985) Topographic and Gravimetric Survey of Samapleu Cupper-Nickel Anomaly. Société pour le Développement Minier de la Côte d'Ivoire, Abidjan, Report No. 518. 12 p.

[6] Djroh, S.P. (2014) Geophysical Studies of the Samapleu Platinum-Bearing Cupronickel de Posit. Essay of 3D Modelling by Interpretation of Magnetic and Electrical Data. PhD Thesis, University Felix Houphouët Boigny, Abidjan, 175 p.

[7] Gouedji, F. (2014) The Samapleu Mafic-Ultramafic Sequences and Their Ni-Cu-EGP Mineralization: A Dyke of the Yacouba Lite Complex; Archean Man Craton, Western Côte d'Ivoire. Unpublished Ph.D. Thesis, Cotutelle, University of Franche Comte-Besançon of France, Université Félix Houphouët-Boigny, Abidjan, 380 p.

[8] Camil, J. (1984) Petrography, Chronology of the Archean Granulite Ensembles and Associated Formations of the Man Region (Côte d'Ivoire). State Thesis, University

of Abidjan, Abidjan, 306 p.

[9] Tagini, B. (1971) Structural Sketch of the Côte d'Ivoire. Regional Geotectonic Essay, State Doctorate Thesis of Natural Sciences, University of Lausanne (Suisse) and SODEMI, Côte d'Ivoire, 302 p.

[10] Roest, W.R., Verhoef, J. and Pilkington, M. (1992) Magnetic Interpretation Using the 3-D Analytic Signal. *Geophysics*, **57**, 116-125. https://doi.org/10.1190/1.1443174

[11] Carignan, J., Hild, P., Mevelle, G., Morel, J. and Yeghicheyan, D. (2001) Routine Analyses of Trace Elements in Geological Samples Using Flow Injection and Low Pressure on-Line Liquid Chromatography Coupled to ICP-MS: A Study of Geochemical Reference Materials BR, DR-N, UB-N, AN-G and GH. *Geostandards Newsletter*, **25**,187-198. https://doi.org/10.1111/j.1751-908X.2001.tb00595.x

[12] Gouedji, F., Picard, C., Coulibaly, Y., Audet, M.A., Auge, T., Goncalves, P., Paquette, J.-L. and Ouattara, N. (2014) The Samapleu Mafic-Ultramafic Intrusion and Its Ni-Cu-PGE Mineralization: An Eburnean (2.09 Ga) Feeder Dyke to the Yacouba Layered Complex (Man Archean Craton, Western Côte d'Ivoire). *Bulletin de la Société Géologique de France* **185**, 393-411. https://doi.org/10.2113/gssgfbull.185.6.393

[13] Rollinson, H.R. (1993) Using Geochemical Data: Evaluation, Presentation, Interpretation. Longman Scientific and Technical, Wiley, New York, 352 p. https://doi.org/10.1180/minmag.1994.058.392.25

[14] Evensen, N.M., Hamilton, P.J. and O'nions, R.K. (1978) Rare Earth Abundances in Chondritic Meteorites. *Geochimica et Cosmochimica Acta*, **42**, 1199-1212. https://doi.org/10.1016/0016-7037(78)90114-X

[15] Esmel, W. (2019) Petrographic and Structural Characterisation of the Contact between the Yepleu Mafic-Ultramafic Intrusion and the Archean Basement (Man Craton, Côte d'Ivoire). Unpublished Master of Geology, Université Félix Houphouët-Boigny, Abidjan, 55 p.

[16] Kouamelan, A.N., Delor, C. and Peucat, J.J. (1997) Geochronological Evidence for Reworking of Archaean Terrains during the Early Proterozoic (2.1 Ga) in the Western Côte d'Ivoire (Man Rise - West African Craton). *Precambrian Research*, **86**, 177-199. https://doi.org/10.1016/S0301-9268(97)00043-0

[17] Caby, R., Delor, C. and Agoh, O. (2000) Lithology and Metamorphism of the Birimian for Mations in the Odienné Region (Côte d'Ivoire): Major Role of Diapirism of the Plutons and of Detachments at the Edge of the Man Craton. *Journal of African Earth Science*, **30**,351-374. https://doi.org/10.1016/S0899-5362(00)00024-5

[18] Pronost, J. (2005) Effects of Continental Contamination and Fluid-Rock Interactions on the Platreef. Bushveld Igneous Complex, South Africa. PhD Thesis, Blaise Pascal Clermont Ferrand II University, Aubière, 258 p.

[19] Pitra, P., Kouamelan, A.N., Ballevre, M. and Peucat, J.J. (2010) Paleoproterozoic High-Pressure Granulite Overprint of the Archean Continental Crust: Evidence for Homogeneous Crustal Thickening (Man Rise, Ivory Coast). *Journal of Metamorphic Geology*, **28**, 41-58. https://doi.org/10.1111/j.1525-1314.2009.00852.x

[20] Baptiste, J. (2013) Structural Characterization and Pressure-Temperature Evolution of Archean-Paleoproterozoic Assemblages of the Man Craton Biankouma Area. Master of Applied Geology, University of Franche-Comté, Côte d'Ivoire, 31 p.

[21] Hagemann, R. and Treuil, M. (1998) Introduction to Geochemistry and Its Applications; Volume 1: Concepts and Methods, Chemical Zonation of the Planet. Commissariat à l'Energie Atomique (CEA), Paris and Gif-sur-Yvette, 445 p.

[22] Kouamelan, A.N. (1996) Geochronology and Geochemistry of the Archean and

Proterozoic Formations of the Man Ridge in Côte d'Ivoire. Implication for the Archean-Proterozoic Transition. Unique PhD Thesis, Geosciences University of Rennes 1, Rennes, 167 p.

[23] Martin, H. and Moyen, J.F. (2002) Secular Changes in TTG Composition as Markers of the Progressive Cooling of the Earth. *Geology*, **30**, 319-322. https://doi.org/10.1130/0091-7613(2002)030%3C0319:SCITTG%3E2.0.CO;2

[24] Diaby, A.J. (2022) Petrography of the Bounta Formations (Biankouma, West of Côte d'Ivoire). Unpublished Master of Geology, Université de Man, Côte d'Ivoire, 40 p.

[25] Gonho, B.A. (2022) Petrography of the Mafic Rocks of Bounta (Biankouma, Western Côte d'Ivoire). Unpublished Master of Geology, University of Man, Côte d'Ivoire, 39 p.

[26] Gouedji, G.E.F., Audet, M-A., Coulibaly, Y., Picard, C., Ouattara, N. and Bakayoko, B. (2018) Contribution of Mineralogy and Crystallochemistry to the Knowledge of the Emplacement Conditions of the Ni-Cu-EGP Mafic-Ultramafic Intrusion of Samapleu (Yacouba Unit Complex, Western Côte d'Ivoire). *Revue Africaine et Malgache de Recherche Scientifique*, **6**, 49-67.

[27] Borisova, A. Yu., Belyatsky, B.V., Portnyagin, M.V. and Sushchevskaya, N.M. (2001) Petrogenesis of Olivine-Phyric Basalts from the Aphanasey Nikitin Rise: Evidence for Contamination by Cratonic Lower Continental Crust. *Journal of Petrology*, **42**, 277-319. https://doi.org/10.1093/petrology/42.2.277

[28] Li, X.H., Su, L., Chung, S., Li, Z.X., Liu, Y., Song, B. and Liu, D.Y. (2005) Formation of the Jinchuan Ultramafic Intrusion and the World's Third Largest Ni-Cu Sulfide Deposit: Associated with the ~825 Ma South China Mantle Plume. *Geochemistry Geophysics Geosystems*, **6**, Q11004. https://doi.org/10.1029/2005GC001006

[29] Lehmann, J., Arndt, N., Windley, B., Mei-Fu, Z., Yan, W.C. and Harris, C. (2007) Field Relationships and Geochemical Constraints on the Emplacement of the Jinchuan Intrusion and Its Ni-Cu-PGE Deposit Gansu, China. *Economic Geologists*, **102**, 75-94. https://doi.org/10.2113/gsecongeo.102.1.75

[30] Gouedji, F., Picard, C., Audet, M.-A., Goncalves, P., Coulibaly, Y. and Bakayoko, B. (2021) The Samapleu Mafic-Ultramafic Intrusion (Western Côte d'Ivoire): Cumulate of a High-Mg Basaltic Magma with (Coeval) Ultrahigh-Temperature-Medium-Pressure Metamor Phism. In: Aïfa, T., Ed., *Mineralization and Sustainable Development in the West African Craton*: *From Field Observations to Modelling*, Geological Society of London, London, 251-282. https://doi.org/10.1144/SP502-2019-130

[31] Arndt, N.T., Lesher, C.M. and Czamanske, G.K. (2005) Mantle-Derived Magmas and Magmatic Ni-Cu-(PGE) Deposits. In: Hedenquist, J.W., Thompson, J.F.H., Goldfarb, R.J. and Richards, J.P., Eds., *Society of Economic Geologists* 100*th Anniversary Volume*, Society of Economic Geologists, Littleton, 5-23. https://doi.org/10.5382/AV100.02

[32] Barnes, S.J. and Robertson, J.C. (2019) Time Scales and Length Scales in Magma Flow Pathways and the Origin of Magmatic Ni-Cu-PGE Ore Deposits. *Geoscience Frontiers*, **10**, 77-87. https://doi.org/10.1016/j.gsf.2018.02.006

[33] Gouedji, F., Picard, C., Audet, M-A., Auge, T. and Spangenberg, J. (2021) Ni-Cu Sul Phide Mineralization and PGM from the Samapleu Mafic-Ultramafic Intrusion, Yacouba Complex, Western Côte d'Ivoire. *The Canadian Mineralogist*, **59**, 631-665. https://doi.org/10.3749/canmin.1900030